# Local Structure and Near-Infrared Emission Features of Neodymium-Based Amine Functionalized Organic/Inorganic Hybrids

**M. C. Gonçalves,[†] N. J. O. Silva,[‡] V. de Zea Bermudez,*[,†] R. A. Sá Ferreira,[‡] L. D. Carlos,[‡] K. Dahmouche,[§] C. V. Santilli,[§] D. Ostrovskii,[||] I. C. Correia Vilela,[†] and A. F. Craievich[⊥]**

*Departamento de Química and CQ-VR, Universidade de Trás-os-Montes e Alto Douro, 5000-911 Vila Real, Portugal, Departamento de Física and CICECO, Universidade de Aveiro, 3810-193 Aveiro, Portugal, Instituto de Química/UNESP, C. P. 355, 14800-900 Araraquara, Brazil, Instituto de Física/USP, São Paulo-SP, Brazil, and Department of Applied Physics, Chalmers University of Technology, 41296 Göteborg, Sweden*

*Received: April 22, 2005; In Final Form: August 29, 2005*

$Nd^{3+}$-based organic/inorganic hybrids have potential application in the field of integrated optics. Attractive sol−gel derived di-urea and di-urethane cross-linked poly(oxyethylene) (POE)/siloxane hybrids (di-ureasils and di-urethanesils, respectively) doped with neodymium triflate ($Nd(CF_3SO_3)_3$) were examined by Fourier transform mid-infrared (FT-IR), Raman (FT-Raman), $^{29}Si$ magic-angle spinning (MAS) nuclear magnetic resonance (NMR) and photoluminescence spectroscopies, and small-angle X-ray scattering (SAXS). The goals of this work were to determine which cation coordinating site of the host matrix (ether oxygen atoms or carbonyl oxygen atoms) is active in each of the materials analyzed, its influence on the nanostructure of the samples and its relation with the photoluminescence properties. The main conclusion derived from this study is that the hydrogen-bonded associations formed throughout the materials play a major role in the hybrids nanostructure and photoluminescence properties.

## Introduction

Recent studies on sol−gel[1] derived hybrids[2] incorporating rare-earth (RE) ions have demonstrated the technological potential of these materials in the domain of optics, specially for the fabrication of displays and lighting devices.[3] In these organic/inorganic matrices, usually designated as ORMOSILS (organically modified silicates), the thermal and mechanical stability of a siloxane-type network are combined with the elastomeric character provided by the organic segments. The desirable characteristics of polymers, namely the easy processability into films, are thus brought together in a single material with the optical features provided by the luminescent centers. In addition, the transparency of xerogel samples, a fundamental requirement for optical applications, is significantly better than that observed with films based on commercial polymers including the same guest species.

In the field of integrated optics (IO) there is substantial interest in the infrared emission of hybrids incorporating RE active centers.[4] Although optical amplification might in principle be obtained in $Nd^{3+}$- or $Er^{3+}$-based materials for IO devices, the high multiphonon decay rates of RE excited states (specially deactivations associated with O−H oscillators) observed in the hybrid hosts proposed have delayed the practical application of such systems.[5−14]

The di-urea and di-urethane cross-linked poly(oxyethylene) (POE)/siloxane hybrid host frameworks are good candidates to minimize nonradiative paths, because they are essentially nonhygroscopic and display excellent encapsulating ability toward guest RE ions.These hybrid matrices, named di-ureasils and di-urethanesils, were represented by the notations d-U(*Y*) and d-Ut(*Y*′), respectively, where d denotes di, U and Ut indicate the urea (−NHC(=O)NH−) and urethane (−NH(C=O)O−) cross-links, respectively, and *Y* and *Y*′ are the average molecular weight of the POE chains in $g \cdot mol^{-1}$. We demonstrated that the $Nd^{3+}$-doped d-U(*Y*) (*Y* = 900 and 2000, corresponding to approximately to 15.5 and 40.5 oxyethylene ($CH_2CH_2O$) repeat units, respectively) di-ureasils combine at room temperature (RT) the cation near-infrared emission (700−1400 nm), assigned to the $^4F_{3/2} \rightarrow {}^4I_{9/2,11/2,13/2}$ intra-$4f^3$ transitions, with the host hybrid purple-blue-green emission (350−570 nm), associated with the siliceous backbone and with the NH groups of the urea bridges.[9,10] We also reported the existence of visible-to-infrared energy conversion in the same systems, resulting from energy transfer processes between the host and the cation.[10]

In the present work we perform an in-depth FT-IR, FT-Raman, photoluminescence, and $^{29}Si$ MAS NMR spectroscopic and SAXS investigation on d-U(600)-based di-ureasils (approximately 8.5 $CH_2CH_2O$ repeat units) and d-Ut(300)- and d-Ut(600)- based di-urethanesils (approximately 6 and 13 $CH_2CH_2O$ repeat units, respectively) doped with a wide range of $Nd(CF_3SO_3)_3$ concentration. The main goals of this study were: (1) to determine how the doping content, the polymer chain length and the nature of the cross-links affect the coordination process of the lanthanide ions; (2) to elucidate the cation coordination/nanostructure/photoluminescence properties relationship. We must emphasize that there are three available coordinating sites for the cations in these POE/siloxane hybrid frameworks: (1) the ether oxygen atoms of the polymer chains, (2) the carbonyl oxygen atoms of the cross-links, and (3) the triflate oxygen atoms.[15−18]

* Corresponding author. Telephone: +351-259-350253. Fax: +351-259-350480. E-mail: vbermude@utad.pt.
[†] Universidade de Trás-os-Montes e Alto Douro.
[‡] Universidade de Aveiro.
[§] Instituto de Química/UNESP.
[⊥] Instituto de Física/USP.
[||] Chalmers University of Technology.

10.1021/jp052097n CCC: $30.25 
Published on Web 10/07/2005

**TABLE 1: Correspondence between Salt Composition ($n$, Where $n$ = moles of $OCH_2CH_2$/moles of $Nd^{3+}$) and Nd Content (wt % Nd, where wt % Nd = $w_{Nd}/w_{Sample} \times 100$) for d-U(600)$_n$Nd($CF_3SO_3$)$_3$ Di-ureasils and d-Ut(300)$_n$Nd($CF_3SO_3$)$_3$ and d-Ut(600)$_n$Nd($CF_3SO_3$)$_3$ Di-urethanesils**

| | d-U(600)$_n$Nd($CF_3SO_3$)$_3$ | | | | | d-Ut(300)$_n$Nd($CF_3SO_3$)$_3$ | | | | | d-Ut(600)$_n$Nd($CF_3SO_3$)$_3$ | | | | |
|---|---|---|---|---|---|---|---|---|---|---|---|---|---|---|---|
| $n$ | $m_{salt}$ (g) | $m$(Nd) (g) | Si/$Nd^{3+}$ (mol $mol^{-1}$) | Si/$Nd^{3+}$ (g $g^{-1}$) | $x$ | $m_{salt}$ (g) | $m$(Nd) (g) | Si/$Nd^{3+}$ (mol $mol^{-1}$) | Si/$Nd^{3+}$ (g $g^{-1}$) | $x$ | $m_{salt}$ (g) | $m$(Nd) (g) | Si/$Nd^{3+}$ (mol $mol^{-1}$) | Si/$Nd^{3+}$ (g $g^{-1}$) | $x$ |
| 400 | 0.031 | 0.008 | 94.12 | 18.33 | 0.0028 | | | | | | | | | | |
| 200 | 0.063 | 0.015 | 47.06 | 9.16 | 0.0055 | 0.095 | 0.023 | 62.41 | 12.15 | 0.0057 | 0.098 | 0.024 | 30.24 | 5.89 | 0.0084 |
| 100 | 0.126 | 0.031 | 23.53 | 4.58 | 0.0107 | 0.190 | 0.046 | 31.21 | 6.08 | 0.0111 | 0.196 | 0.048 | 15.12 | 2.94 | 0.0163 |
| 80 | 0.157 | 0.038 | 18.82 | 3.67 | 0.0132 | 0.237 | 0.058 | 24.96 | 4.86 | 0.0137 | 0.245 | 0.060 | 12.10 | 2.36 | 0.0200 |
| 60 | | | | | | 0.316 | 0.077 | 18.72 | 3.65 | 0.0180 | 0.326 | 0.080 | 9.07 | 1.77 | 0.0260 |
| 40 | 0.314 | 0.077 | 9.41 | 1.83 | 0.0251 | | | | | | | | | | |
| 20 | 0.628 | 0.153 | 4.71 | 0.92 | 0.0456 | 0.948 | 0.231 | 6.24 | 1.22 | 0.0470 | 0.978 | 0.239 | 3.02 | 0.59 | 0.0642 |
| 10 | 1.257 | 0.307 | 2.35 | 0.46 | 0.0768 | 1.895 | 0.462 | 3.12 | 0.61 | 0.0788 | 1.956 | 0.477 | 1.51 | 0.29 | 0.1016 |
| 5 | 2.514 | 0.613 | 1.18 | 0.23 | 0.1168 | 3.791 | 0.924 | 1.56 | 0.30 | 0.1191 | 3.912 | 0.954 | 0.76 | 0.15 | 0.1435 |

## Experimental Section

**Sample Preparation. Materials.** 3-Isocyanatepropyltriethoxysilane (ICPTES, Fluka) and Nd($CF_3SO_3$)$_3$ (Aldrich) were used as received. Poly(ethylene glycol)s (PEG(300) and PEG(600), Aldrich, $M_w \approx 300$ and 600 g $mol^{-1}$, respectively), $\alpha,\beta$-diaminepoly(oxyethylene-*co*-oxypropylene) glycol (commercially designated as Jeffamine 600, Fluka, $M_w \approx 600$ g·$mol^{-1}$), tetrahydrofuran (THF, Merck) and ethanol ($CH_3CH_2OH$, Merck) were stored over molecular sieves. High purity distilled water was used in all experiments.

**Synthesis of the d-U(600)$_n$Nd($CF_3SO_3$)$_3$ and d-Ut(300)$_n$Nd($CF_3SO_3$)$_3$ Xerogels.** The synthesis of the d-U(600)-based di-ureasils and that of the d-Ut(300)-based di-urethanesils incorporating Nd($CF_3SO_3$)$_3$ was performed according to the procedure described earlier for di-ureasil analogues doped with other lanthanide triflates[19] and di-urethanesil analogues doped with europium triflate,[18] respectively. In agreement with the designation used previously,[18,19] the di-ureasils and the di-urethanesils obtained here were identified by the formula d-U(600)$_n$Nd($CF_3SO_3$)$_3$ and d-Ut(300)$_n$Nd($CF_3SO_3$)$_3$ where $n$ represents the number of $OCH_2CH_2$ units per $Nd^{3+}$ ion. Xerogel samples of di-ureasils and di-urethanesils with $\infty \geq n \geq 5$ were prepared. This range of compositions corresponds to $Nd^{3+}$ concentration ranges of $0 \leq x \leq 0.1168$ and $0 \leq x \leq 0.1191$, respectively, where $x$ represents the $Nd^{3+}$ mass per total mass of sample (Table 1).

**Synthesis of the d-Ut(600)$_n$Nd($CF_3SO_3$)$_3$ Xerogels.** The first stage of the synthesis of the d-Ut(600)-based di-urethanesils involved the formation of covalent urethane linkages between the terminal hydroxyl groups of PEG(600) and the isocyanate groups of the alkoxysilane precursor ICPTES. In the second stage of the synthesis water and $CH_3CH_2OH$ were added to promote the hydrolysis and condensation reactions characteristic of the sol−gel process. The guest salt was added in the latter step.

**Step 1. Synthesis of the Di-urethanesil Hybrid Precursor, d-UtPTES(600).** A 1.5 g sample of PEG(600) was dissolved in 10 mL of THF by magnetic stirring. A volume of 1.234 mL of ICPTES was added to this solution in a fume cupboard (molar proportion 2:1 ICPTES:PEG(600)). The flask was then sealed and the solution stirred for 24 h at moderate temperature (approximately 70 °C). The grafting process was infrared monitored. During the formation of the urethane cross-links the intensity of the prominent and sharp absorption band located at 2273 $cm^{-1}$, ascribed to the stretching vibration of the isocyanate group of the $\equiv Si-(CH_2)_3-N=C=O$ moiety, progressively decreased, until it disappeared upon completion of the reaction. These spectral changes were accompanied by the growth of a series of new bands produced by the urethane group in the 1760−1530 $cm^{-1}$ spectral region.

**Step 2. Synthesis of the Di-urethanesil Hybrid Xerogels, d-Ut(600)$_n$Nd($CF_3SO_3$)$_3$.** A volume of 1.169 mL of $CH_3CH_2OH$, an appropriate mass of Nd($CF_3SO_3$)$_3$ (Table 1), and 135 $\mu$L of water were added to the d-UtPTES(600) solution prepared in the first stage of the synthetic procedure (molar proportion 1:4:1.5 ICPTES:$CH_3CH_2OH$:$H_2O$). The mixtures were stirred in a sealed flask for 30 min and then cast into a Teflon mold which was covered with Parafilm and left in a fume cupboard for 24 h. After a few hours, gelation was already visible. The mold was transferred to an oven at 60 °C and the sample was aged for a period of 2 weeks. A transparent monolithic bulk was thus formed. Samples with $n = \infty$, 200, 100, 80, 60, 20, 10, and 5 were prepared (Table 1).

## Experimental Techniques

**FT-IR Spectroscopy.** FT-IR spectra were acquired at RT using a Bruker 22 (Vektor) spectrometer placed inside a glovebox with a dry argon atmosphere. The spectra were collected over the 4000−400 $cm^{-1}$ range by averaging 150 scans at a spectral resolution of 2 $cm^{-1}$. Solid samples (2 mg) were finely ground, mixed with approximately 175 mg of dried potassium bromide (Merck, spectroscopic grade) and pressed into pellets. Prior to recording the spectra, the pellets were first vacuum-dried at 80−90 °C for about 60 h, to reduce the levels of adsorbed water and solvent, and then transferred into a glovebox.

**FT-Raman Spectroscopy.** The FT-Raman spectra were recorded at RT with a Bruker IFS-66 spectrometer equipped with a FRA-106 Raman module and a near-infrared YAG laser with wavelength 1064 nm. The spectra were collected over the 3200−300 $cm^{-1}$ range at a resolution of 2 $cm^{-1}$. The accumulation time for each spectrum was 4 h.

To evaluate complex band envelopes and to identify underlying spectral components, the iterative least-squares curve-fitting procedure in the PeakFit[20] software was used extensively throughout this study. The best fit of the experimental data was obtained by varying the frequency, bandwidth, and intensity of the bands. The standard errors of the curve-fitting procedure were less than 0.007. Taking into account the morphology of materials under investigation we decided to employ Gaussian band shapes. Disordering in a system, which causes statistical distribution of the oscillators, may explain why the experimental band shapes are very often changed from the natural Lorentzian shape to the Gaussian form. Thus, typical band profiles observed in solid disordered materials are rather Gaussian. Although it is in general accepted that in such cases the peaks are best fitted with a Voigt shape (a mixture of Lorentzian and Gaussian contributions), the use of this function is not straightforward and may lead to ambiguous results due to the possibility of different Gaussian−Lorentzian proportions.

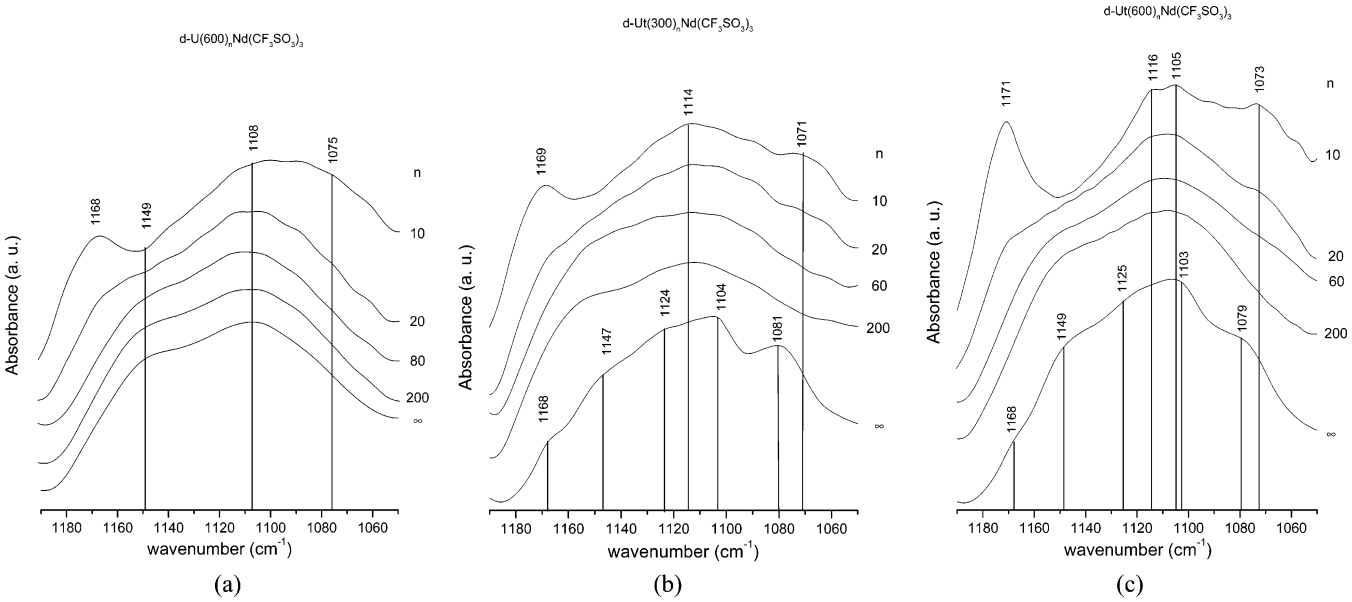


**Figure 1.** RT FT-IR spectra in the $\nu_{COC}$ region of the selected (a) d-U(600)$_n$Nd(CF$_3$SO$_3$)$_3$ di-ureasils and (b) d-Ut(300)$_n$Nd(CF$_3$SO$_3$)$_3$ and (c) d-Ut(600)$_n$Nd(CF$_3$SO$_3$)$_3$ di-urethanesils.

**$^{29}$Si MAS NMR Spectroscopy.** $^{29}$Si MAS NMR spectra were recorded on a Bruker Avance 400 (9.4 T) spectrometer at 79.49 MHz with 2 $\mu$s (equivalent to 30°) rf pulses, a recycle delay of 60 s and at a 5.0 kHz spinning rate. Chemical shifts are quoted in ppm from tetramethylsilane (TMS).

**SAXS.** The X-ray scattering measurements were performed at the National Synchrotron Light Laboratory (LNLS), Campinas, Brazil, using its SAXS beamline which provides a monochromatic ($\lambda = 1.608$ Å) and horizontally focused beam. The intensity was recorded as a function of the modulus of the scattering vector $q$ (where $q = (4\pi/\lambda)\sin(\epsilon/2)$, $\epsilon$ being the scattering angle). Because of the small size of the incident beam cross section at the detection plane, no mathematical desmearing of the experimental SAXS intensity was needed. Each spectrum corresponds to a data collection period of 300s. The relative error of the SAXS intensity evaluated from the statistical variance associated with the number $N_f$ of photons collected during data acquisition, is $\Delta I(q)/I(q) = 2/N_f^{1/2}$. The relative error was significant only over the high $q$ scattering intensities. The parasitic scattering intensity from air, slits, and windows was subtracted from the total intensity. The scattering intensity was also normalized by taking into account the varying intensity of the direct X-ray beam, sample absorption and sample thickness.

**Photoluminescence Spectroscopy.** The RT emission (PL) and excitation (PLE) spectra were detected in the visible spectral range on a modular double grating excitation spectrofluorimeter with a TRIAX 320 emission monochromator (Fluorolog-3, Jobin Yvon-Spex) coupled to a R928 Hamamatsu photomultiplier, in the front face acquisition mode. All the photoluminescence spectra were corrected for optics and detection spectral response. The RT infrared PL spectra were recorded on a Bruker IFS 66v Fourrier transform infrared (FT-IR) coupled to a Ge North-Coast EO-817 photodiode cooled to 77 K. The 514.5 nm line of an Ar ion-laser was used as excitation source.

## Results and Discussion

**FT-IR, FT-Raman, and NMR Spectroscopies. Cation/Polymer Interaction.** To probe the coordination of the $Nd^{3+}$ ions by the ether oxygen atoms of the POE chains in the doped d-U(600)-, d-Ut(300)- and d-Ut(600)-based samples, we will seek in the region characteristic of the skeleton COC stretching ($\nu_{COC}$) modes (1190−1050 cm$^{-1}$ interval) spectral changes resulting from the addition of increasing amounts of the lanthanide salt. In this range of wavenumbers the interaction between the cations and the polymer ether oxygen atoms is manifested through a shift of the intense $\nu_{COC}$ band to lower frequencies.[16−18,21−24]

Parts a−c of Figure 1 show the RT FT-IR spectra of selected d-U(600)$_n$Nd(CF$_3$SO$_3$)$_3$ di-ureasils and d-Ut(300)$_n$Nd(CF$_3$SO$_3$)$_3$ and d-Ut(600)$_n$Nd(CF$_3$SO$_3$)$_3$ di-urethanesils in the $\nu_{COC}$ region. The broad $\nu_{COC}$ envelope of d-U(600) displays a band at 1108 cm$^{-1}$ and a shoulder at 1149 cm$^{-1}$ (Figure 1a), assigned to the $\nu_{COC}$ mode and to the coupled $\nu_{COC}$ and $CH_2$ rocking ($r_{CH_2}$) modes, respectively.[25,26] Both modes, produced by noncoordinated, disordered POE chains,[25,26] remain unchanged in the presence of guest salt. The feature that emerges around 1075 cm$^{-1}$ in the FT-IR spectra of the d-U(600)$_n$Nd(CF$_3$SO$_3$)$_3$ sample with $n = 10$ is attributed to $Nd^{3+}$-coordinated ether oxygen atoms (Figure 1a).[16−18,21−24] The relative intensity between the 1108 and 1075 cm$^{-1}$ events suggests that the fraction of complexed POE chains is about the same as that of the noncomplexed chains.

In the $\nu_{COC}$ region of the nondoped d-Ut(300) and d-Ut(600) matrices five features centered at about 1168, 1148, 1125, 1104, and 1080 cm$^{-1}$ are identified (Figure 1, parts b and c), an indication that the POE segments are locally ordered.[27] Upon addition of the guest salt to the d-Ut(300) matrix, a very strong $\nu_{COC}$ band emerges near 1114 cm$^{-1}$ and a shoulder, due to the coupled $\nu_{COC}/r_{CH_2}$ modes, develops at approximately 1141 cm$^{-1}$ (Figure 1b).[25,26] The FT-IR spectra of the d-Ut(300)$_n$Nd(CF$_3$SO$_3$)$_3$ with $n \leq 20$ exhibit the feature characteristic of $Nd^{3+}$/POE interaction[16−18,21−24] near 1071 cm$^{-1}$ (Figure 1b). The relative intensity between the 1114 cm$^{-1}$ and the 1071 cm$^{-1}$ bands suggests that, similarly to what happens in the case of the d-U(600)-based analogues discussed above, the fraction of noncoordinated POE chains is about the same as that of the coordinated ones. In the FT-IR spectra of the long chain d-Ut(600)$_n$Nd(CF$_3$SO$_3$)$_3$ compounds with $n = 200$ and 60, we note the presence of the pair of events associated with the occurrence of amorphous POE chains at 1109 and 1141 cm$^{-1}$.[25,26] Figure 1c demonstrates that the further incorporation of Nd(CF$_3$SO$_3$)$_3$ into the d-Ut(600) framework ($n \leq 20$) has

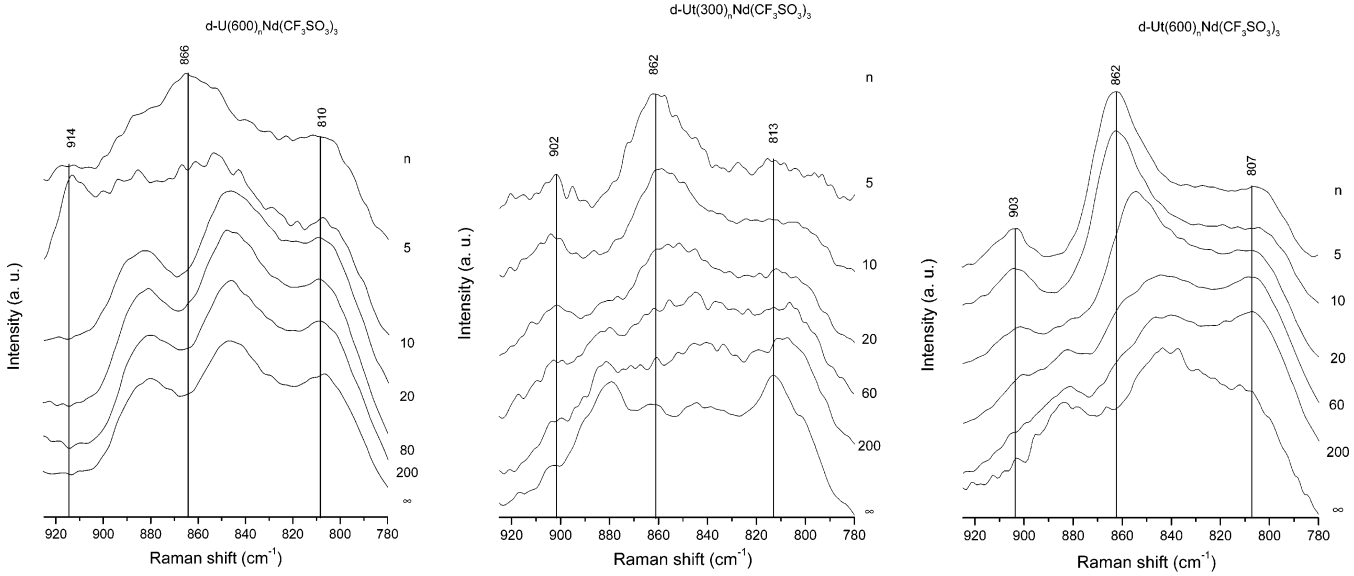


**Figure 2.** RT FT-Raman spectra in the 925−775 cm$^{-1}$ region of the selected (a) d-U(600)$_n$Nd(CF$_3$SO$_3$)$_3$ di-ureasils and (b) d-Ut(300)$_n$Nd(CF$_3$SO$_3$)$_3$ and (c) d-Ut(600)$_n$Nd(CF$_3$SO$_3$)$_3$ di-urethanesils.

tremendous implications in the $\nu_{COC}$ band profile: (1) a shoulder is detected at about 1073 cm$^{-1}$; (2) the very intense 1109 cm$^{-1}$ band is replaced by two strong features observed at 1116 and 1105 cm$^{-1}$. The growth of the 1073 cm$^{-1}$ event provides evidence that in these materials the coordination of the oxygen atoms of the POE segments to the lanthanide ions takes place in the same concentration range as that of the lower molecular weight d-Ut(300)$_n$Nd(CF$_3$SO$_3$)$_3$ analogues.[16−18,21−24] The 1116 and 1105 cm$^{-1}$ bands are attributed to the formation of a salt-rich crystalline POE/Nd(CF$_3$SO$_3$)$_3$ complex.[16]

We must note that the events situated at 1168, 1169, and 1171 cm$^{-1}$ observed in the FT-IR spectra shown in Figure 1, parts a−c, respectively, whose intensity increases with salt addition, are assigned to the asymmetric stretching mode of the $CF_3$ group ($\nu_{a(CF_3)}$) of cation-coordinated $CF_3SO_3^-$ ions.[17,28]

Proofs of the reconfiguration undergone by the POE segments as a result of their interaction with the $Nd^{3+}$ cations can be retrieved from the RT FT-Raman spectra of selected d-U(600)$_n$Nd(CF$_3$SO$_3$)$_3$ di-ureasils and d-Ut(300)$_n$Nd(CF$_3$SO$_3$)$_3$ and d-Ut(600)$_n$Nd(CF$_3$SO$_3$)$_3$ di-urethanesils in the 925−780 cm$^{-1}$ interval (usually called the $r_{CH_2}$ region, which includes a mixture of $r_{CH_2}$ and $\nu_{COC}$ modes) (Figure 2, parts a−c, respectively).

Figure 2a reveals that in this spectral interval the FT-Raman signature of the d-U(600)$_n$Nd(CF$_3$SO$_3$)$_3$ di-ureasils with $200 \geq n \geq 20$ is essentially identical to that of the nondoped matrix. In contrast, the xerogels with $n = 10$ and 5 display a quite different behavior (Figure 2a). The intense band situated at about 866 cm$^{-1}$ in the FT-Raman spectra of both samples is associated with a stretching vibration mode involving wrapping of the POE chains around the $Nd^{3+}$ ion.[29−34] The growth of this mode ("oxygen breathing mode"), characteristic of a gauche conformation of the polymer O−C−C−O bonds,[29−34] indicates that the $Nd^{3+}$ ions interact with the POE ether oxygen atoms at $n \leq 10$. As the formation of the cation/ether oxygen complex favors a gauche conformation of the −O−C−C−O− bonds,[29−32] the intensity of the 810 cm$^{-1}$ band, indicative of the trans conformations of the −O−C−C−O− sequences[29−34] is, as expected, progressively reduced with the increase of salt concentration (Figure 3a). The 914 cm$^{-1}$ band in the FT-Raman spectra of the two most concentrated d-U(600)-based di-ureasil samples is an additional proof of $Nd^{3+}$/POE bonding.[16,32]

The FT-Raman spectra of the d-Ut(300) and d-Ut(600)-based di-urethanesil xerogels with $n \leq 20$ exhibit the "oxygen breathing" mode at about 862 cm$^{-1}$ (Figure 2, parts b and c, respectively). The features located at ca. 902 and 903 cm$^{-1}$ in the same spectra, respectively, corroborate the claim that the coordination of the cations to the POE chains occurs in this high concentration range. The band associated with the trans conformations is discerned in the FT-Raman spectra of the doped d-Ut(300)-and d-Ut(600)-based di-urethanesils at about 813 and 807 cm$^{-1}$, respectively (Figure 2, parts b and c, respectively).

The spectral data presented in this section demonstrate that, while the ether oxygen atoms of the POE segments of the d-U(600)-based di-ureasils start to interact with the $Nd^{3+}$ ions at $n = 10$, the same type of interaction begins already at $n = 20$ in the case of the d-Ut(300) and d-Ut(600)-based di-urethanesils. It is, nevertheless, necessary to stress that the beginning of the participation of the POE chains in the complexation of the $Nd^{3+}$ ions is uncertain, as it may occur at a slightly lower salt concentration. This is due to the fact that the $Nd^{3+}$-coordinated $\nu_{COC}$ band may be masked by the broad noncomplexed $\nu_{COC}$ band. It is also possible that the number of cation-ether oxygen interactions in the more dilute samples is too low to be manifested in the FT-IR or FT-Raman spectra.

To investigate the role played by the triflate oxygen atoms in the cation coordination process we conducted a preliminary FT-IR and FT-Raman spectroscopic analysis of the characteristic symmetric stretching vibration mode of the triflate $SO_3$ group.[35] These studies demonstrated that in the d-U(600)$_n$Nd(CF$_3$SO$_3$)$_3$ di-ureasils with $n > 10$ and in the d-Ut(300)$_n$Nd(CF$_3$SO$_3$)$_3$ and d-Ut(600)$_n$Nd(CF$_3$SO$_3$)$_3$ di-urethanesils with $n > 20$ most of the anions are "free". A minor proportion of weakly coordinated species was also detected. These findings lead us to conclude that in these ranges of salt concentration the coordination of the $Nd^{3+}$ ions to the C═O groups of the cross-links is favored.

**Cation/Cross-Link Interactions.** In this section, we will analyze in depth the spectral signature of the $Nd^{3+}$-doped d-U(600)-based di-ureasils and d-Ut(300)- and d-Ut(600)-based di-urethanesils in the "amide I" region (1800−1600 cm$^{-1}$) to

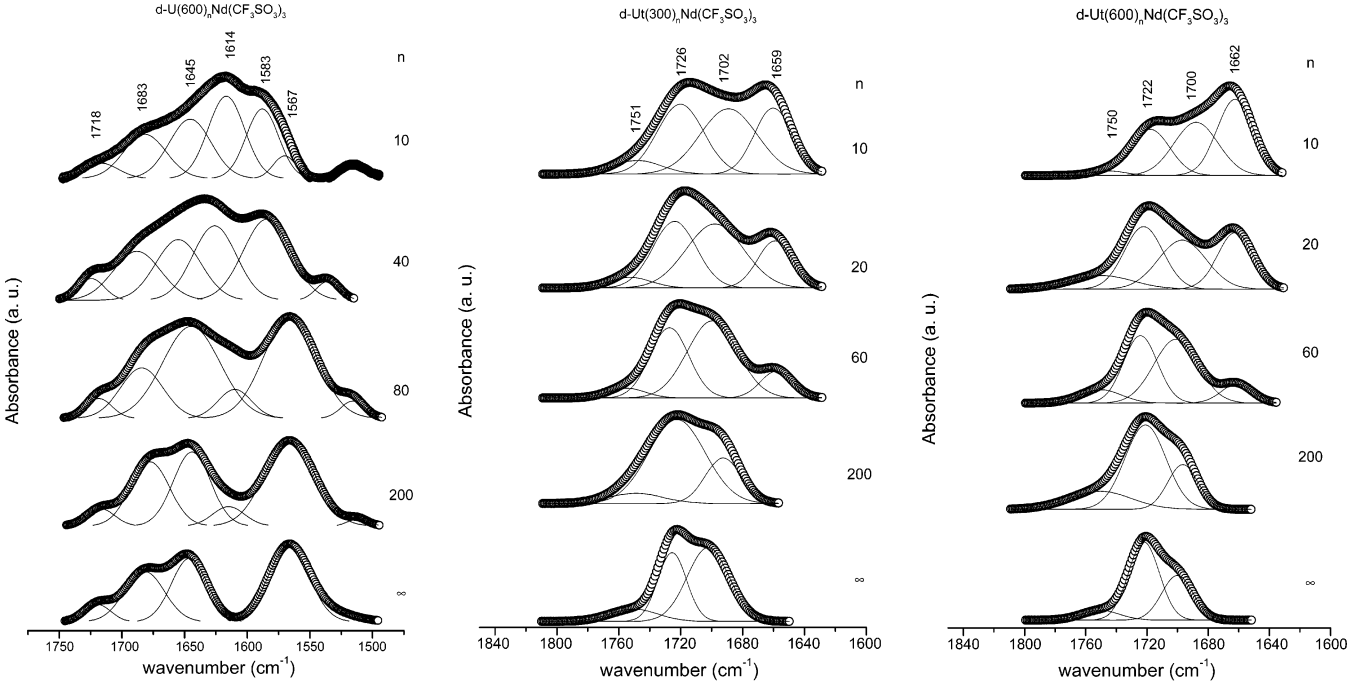


**Figure 3.** Curve-fitting results of the RT FT-IR spectra in the "amide I" region of the selected (a) d-U(600)$_n$Nd(CF$_3$SO$_3$)$_3$ di-ureasils and (b) d-Ut(300)$_n$Nd(CF$_3$SO$_3$)$_3$ and (c) d-Ut(600)$_n$Nd(CF$_3$SO$_3$)$_3$ di-urethanesils. Note: in the case of the di-ureasils, the "amide II" region is also presented.

determine the role played by the carbonyl oxygen atoms of the urea and urethane cross-links, respectively, in the coordination of the $Nd^{3+}$ ions.

The "amide I" mode of the di-ureasils and di-urethanesils corresponds to the amide I mode of polyamides.[36] The amide I mode (or carbonyl stretching mode, $\nu_{C=O}$) is a complex vibration that receives a major contribution from the C═O stretching vibration. As the $\nu_{C=O}$ vibration is sensitive to the specificity and magnitude of hydrogen bonding, the amide I envelope consists of several distinct components which correspond to different environments of the C═O groups, typically called associations, aggregates, or structures. Quantitative analysis is possible in the amide I region only if the difference in the absorption coefficients of the nonbonded and bonded C═O bands is taken into account. Band area calculations may be thus considered as indicative of functional group concentration.[36,37]

To examine the changes that occur in the "amide I" region of the di-ureasils and di-urethanesils as a function of salt concentration, we performed curve-fitting in the 1750−1500 cm$^{-1}$ (Figure 3a) and around 1815−1620 cm$^{-1}$ (Figure 3, parts b and c) envelopes of the corresponding RT FT-IR spectra, assuming Gaussian band shapes. The plots of Figure 4, parts a and b represent the variation of the area of the "amide I" components with composition in the d-Ut(300)$_n$Nd(CF$_3$SO$_3$)$_3$ and d-Ut(600)$_n$Nd(CF$_3$SO$_3$)$_3$ di-urethanesils, respectively. Taking into account the low errors associated with the fitting band parameters (see Experimental Section), the estimated values of the areas are considered to be very accurate. In the case of the d-U(600)-based di-ureasils we could not build this type of plot, since the "amide I" and "amide II" (1600−1500 cm$^{-1}$) regions are superimposed, as illustrated in Figure 3a. As the "amide II" band is a mixed mode containing a major contribution from the N−H in-plane bending vibration,[36] any calculations of the integral area fraction of the components of the band envelope of the di-ureasil samples between 1750 and 1500 cm$^{-1}$ would not give reliable information regarding the C═O environments.

The 1718 and 1683 cm$^{-1}$ features seen in the "amide I" band profile of nondoped d-U(600) are assigned to hydrogen-bonded C═O groups belonging to disordered aggregates (e.g., POE/urea association of structure A) of decreasing strength (Figure 3a).[38] The intense component at 1645 cm$^{-1}$ (Figure 3a) corresponds to the absorption of C═O groups included in much more ordered hydrogen-bonded aggregates (e.g., urea/urea association of structure B).[38]

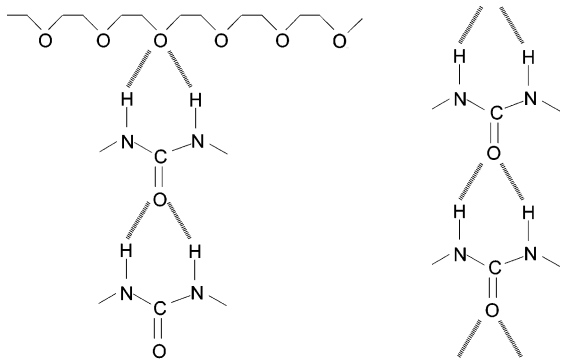


Figure 3a demonstrates that the intensity maxima of the "amide I" envelope of d-U(600) shifts from about 1645 to 1614 cm$^{-1}$ with the increase of salt concentration, a proof that the strength of the hydrogen bonds globally increases. In general terms, the intensity of the 1683 cm$^{-1}$ event is reduced with the progressive addition of Nd(CF$_3$SO$_3$)$_3$. The new "amide I" component that emerges at 1614 cm$^{-1}$ in the xerogel with $n = 200$ (Figure 3a) provides solid evidence that the cations bond strongly to the urea carbonyl oxygen atoms already at very low guest salt concentration. This process is accompanied by the formation of new hydrogen-bonded associations at the expense of the disruption of other initially existent in the host matrix. At $n =$ 10 the new component seen at 1583 cm$^{-1}$ (Figure 3a) is assigned

to an "amide II" component.[38] As this mode is found at 1567 $cm^{-1}$ in the FT-IR spectrum of d-U(600) (Figure 3a),[38] this finding suggests that in some of the hydrogen-bonded aggregates formed at high salt content the hydrogen bonds are considerably stronger[38] than those present in the aggregates detected at lower salt concentration.

The "amide I" envelope of the nondoped d-Ut(300) and d-Ut(600) di-urethanesils is resolved into three distinct components centered at approximately 1751/1750 $cm^{-1}$, 1726/1722 $cm^{-1}$ and 1702/1700 $cm^{-1}$ (Figure 3, parts b and c, respectively). In accordance with previous works[16] the 1751/1750 $cm^{-1}$ feature is attributed to urethane linkages whose N−H and C═O groups are nonbonded (structure C), the 1726/1722 $cm^{-1}$ band is assigned to the absorption of hydrogen-bonded C═O groups included in disordered aggregates (e.g., POE/urethane association of structure D) and the 1702/1700 $cm^{-1}$ event is associated with the absorption of C═O groups belonging to a considerably more ordered hydrogen-bonded aggregate (e.g., urethane/urethane association of structure E).[16]

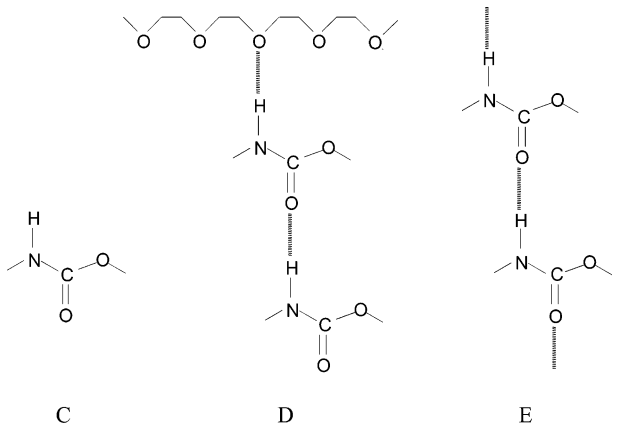

C D E

The integral area fraction of the band inherent to urethane/urethane aggregates (1702/1700 $cm^{-1}$) is considerably greater in the d-Ut(300) matrix than in the d-Ut(600) framework (55% and 34%, respectively) (Figure 4, parts a and b, respectively). In the case of d-Ut(600) the most intense event of the "amide I" region is the 1722 $cm^{-1}$ component (integral area fraction equal to 58%) (Figure 4b). This demonstrates that in the d-Ut(300) matrix the urethane/urethane structures are dominant, whereas in the d-Ut(600) material the POE/urethane associations are preferentially formed. These findings are logical, since the number of urethane cross-links in the d-Ut(300) hybrid is significantly greater than in the long chain d-Ut(600) analogue. In both di-urethanesil matrices the amount of "free" urethane linkages is very low and practically the same (about 10% and 8% in d-Ut(300) and d-Ut(600), respectively) (Figure 4, parts a and b, respectively).

The presence of increasing amounts of the guest neodymium salt in the d-Ut(300) and d-Ut(600) frameworks gives rise to a series of marked changes in the "amide I" region (Figure 3, parts b and c). The intensity maximum of the "amide I" profile of d-Ut(300) and d-Ut(600) shifts from about 1726 to 1659 $cm^{-1}$ (Figure 4b) and from approximately 1722 to 1662 $cm^{-1}$ (Figure 3c), respectively, as the $Nd(CF_3SO_3)_3$ concentration rises, suggesting that the strength of the hydrogen bonds globally increases. In the FT-IR spectra of the d-Ut(300)$_n$Nd$(CF_3SO_3)_3$ and d-Ut(600)$_n$Nd$(CF_3SO_3)_3$ di-urethanesils with $n = 60$ a new band located near 1659/1662 $cm^{-1}$ emerges (Figure 3, parts b and c, respectively) and undergoes a significant increase with the subsequent addition of the lanthanide salt. These spectral

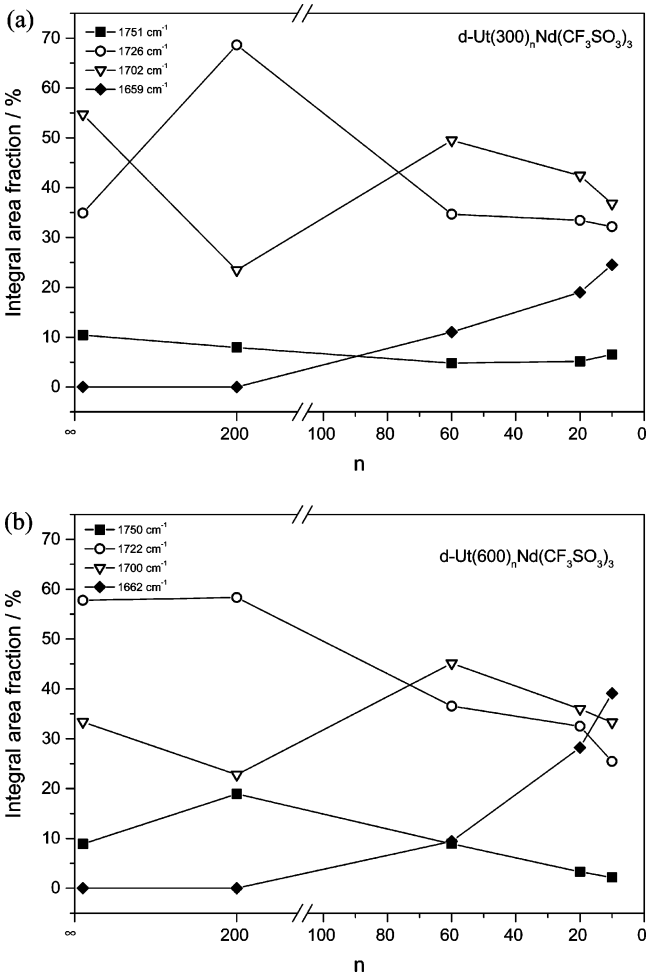


**Figure 4.** Salt concentration dependence of the integral band fraction of the "amide I" bands of the (a) d-Ut(300)$_n$Nd$(CF_3SO_3)_3$ and (b) d-Ut(600)$_n$Nd$(CF_3SO_3)_3$ di-urethanesils. The lines are guide for the eyes.

data demonstrate that the $Nd^{3+}$ ions interact with the carbonyl oxygen atoms of the urethane cross-links within the whole range of concentrations studied.

The plots of Figure 4, parts a and b, show that in the most dilute xerogels analyzed ($n = 200$) the proportion of nonbonded C═O groups (1751/1750 $cm^{-1}$) with respect to the host d-Ut(300) and d-Ut(600) materials suffers minor changes. In parallel, in the d-Ut(300)$_{200}$Nd$(CF_3SO_3)_3$ sample the amount of POE/urethane aggregates (1726/1722 $cm^{-1}$) is dramatically increased (Figure 4a), whereas it remains practically the same in the d-Ut(600)$_{200}$Nd$(CF_3SO_3)_3$ xerogel (Figure 4b). In both di-urethanesils we note that the fraction of urethane/urethane aggregates (1702/1700 $cm^{-1}$) decreases, although this effect is much more pronounced in the case of d-Ut(300)$_{200}$Nd$(CF_3SO_3)_3$ (Figure 4, parts a and b). Upon further addition of $Nd^{3+}$ ions to both matrices ($n = 60$) the proportion of nonbonded C═O groups and POE/urethane aggregates is reduced. The destruction of the latter hydrogen-bonded associations is quite important in the case of the d-Ut(300)-based material (Figure 4a). In both samples, the number of urethane/urethane aggregates increases significantly (Figure 4, parts a and b). Another relevant alteration at $n = 60$ is the growth of a new feature at 1659/1662 $cm^{-1}$ presumably associated with the formation of ordered aggregates with hydrogen bonds stronger than those established in the urethane/urethane associations. Globally, at $n < 60$ the modifications that take place are less marked than in the more dilute materials (Figure 4, part a and b): the fraction of POE/urethane and urethane/urethane structures is subject to a moderate

reduction and the 1659/1662 $cm^{-1}$ band continues to increase. In addition, the proportion of nonbonded C═O groups remains practically unchanged in the d-Ut(300)$_n$Nd$(CF_3SO_3)_3$ materials, suffering a minor decrease in the case of the d-Ut(600)-based analogues. Thus, we are led to conclude that in the salt-rich samples with $n = 20$ and 10 the new ordered aggregates are built at the expense of the destruction of the POE/urethane and urethane/urethane structures.

**Siloxanes Species.** In this section, we will analyze the role played by the $Nd^{3+}$ triflate content in the nature of the polycondensed siloxane species in the di-ureasil and di-urethanesil media by means of $^{29}Si$ NMR/MAS. Typically, the notation $T^i$ represents the number $i$ ($i = 1,2,3$) of connections that each silicon atom makes, through oxygen bridges, with silicon neighbors.

The $^{29}Si$ NMR/MAS spectra of the d-U(600)$_n$Nd$(CF_3SO_3)_3$ ($n = 200$ and 40), d-Ut(300)$_n$Nd$(CF_3SO_3)_3$ ($n = 200$ and 80) and d-Ut(600)$_n$Nd$(CF_3SO_3)_3$ ($n = 200$ and 80) are plotted in Figure 5, parts a−c, respectively. All the spectra exhibit essentially two bands located around −58 and −66 ppm attributed to the presence of $T^2$ ($-CH_2Si(OSi)_2OR$) and $T^3$ ($-CH_2Si(OSi)_3$) species, respectively (where R is $CH_2CH_3$ or H). In the $^{29}Si$ NMR/MAS spectra of the d-U(600)- and d-Ut(300)-based hybrids a small band located around −50 ppm, attributed to the presence of $T^1$ ($-CH_2Si(OSi)(OH)_2$) environments, is seen (Figure 5, parts a and b, respectively). The relative proportion between $T^1$, $T^2$, and $T^3$ species was calculated from the integrated area under the peaks (Table 2). For the d-U(600) and d-Ut(300)-based xerogels the polycondensation degree $c$ (where $c = {}^1/_3(\%T^1 + 2\%T^2 + 3\%T^3)$ has a minor decrease with the $Nd^{3+}$ triflate content. The proportion of $T^2$ and $T^3$ species and consequently the degree of polycondensation is independent of the doping content in the d-Ut(600)-based materials. On the basis of these data, we have deduced the approximate structure of the d-U(600) (where $a + c = 2.5$), d-Ut(300) and d-Ut(600) matrices in the $Nd(CF_3SO_3)_3$-doped materials (structures F, G and H, respectively).

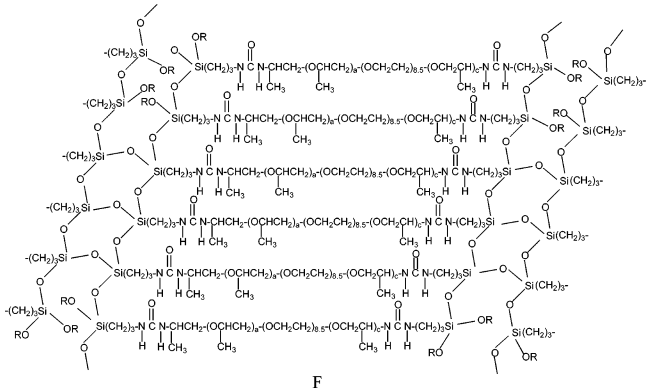

F

**SAXS.** The SAXS intensity curves corresponding to the d-U(600)$_n$Nd$(CF_3SO_3)_3$ ($400 \geq n \geq 40$), d-Ut(300)$_n$Nd-$(CF_3SO_3)_3$ ($200 \geq n \geq 60$), and d-Ut(600)$_n$Nd$(CF_3SO_3)_3$ ($200 \geq n \geq 80$) hybrids are plotted in Figure 6, parts a−c, respectively. The peaks and/or shoulder apparent in the SAXS pattern of the undoped sample, at medium $q$, have been assigned to an interference effect in the X-ray scattering amplitude produced by the existence of spatially correlated siloxane-rich particles embedded in the polymeric-rich phase.[39] Supporting this assignment, it has been verified, as expected, that the $q$ values corresponding to the maximum of the correlation peaks decrease at increasing polymer chain length.[39] In the high $q$ range, the scattering intensity decreases following Porod's law.[40]

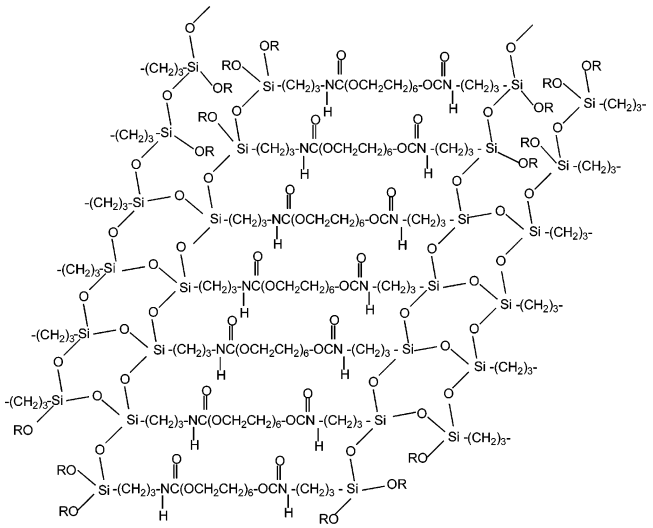

G

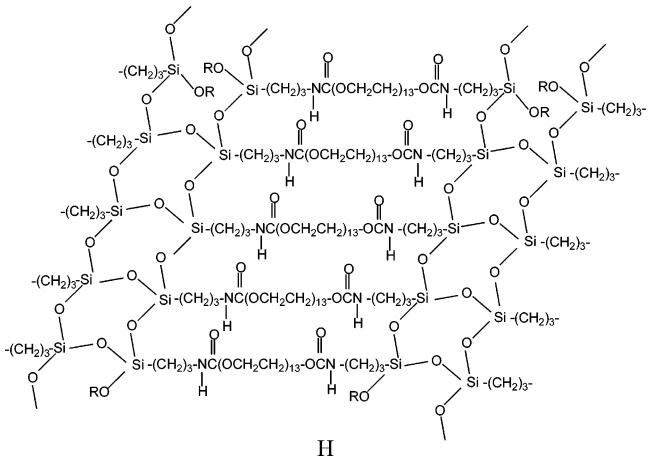

H

For some samples the Porod behavior was not observed within the $q$ range of the SAXS experiments.

All the experimental scattering curves plotted in Figure 6, parts a−c, exhibit, over the very low $q$ region ($q < 0.1$ Å$^{-1}$), a sharp decreasing trend. This decreasing intensity was considered as an additive contribution produced by electron density heterogeneities with a characteristic size much larger than that of siloxane particles (∼200−300 Å). In previously studied and similar systems, these large heterogeneities were associated with a clustering or segregation process of siloxane particles leading to relatively large siloxane-rich domains embedded in a siloxane cluster-depleted matrix.[41,42] In further analysis, we have only taken into account the scattering intensity above 0.1−0.15 Å$^{-1}$, so that the derived information essentially concerns the nanometric structure inside the mentioned domains.

The medium and high $q$ regions of the SAXS curves were analyzed on the basis of the approach described in a previous work concerning similar systems.[41,42] This approach involves the use of a semiempirical equation proposed by Beaucage et al.[43,44] for the scattering intensity produced by a "two electron density" system of isolated particles embedded in a homogeneous matrix that takes into account spatial correlation effects:

$$I(q) = \left\{ G \exp\left(\frac{-q^2 R_g^{\,2}}{3}\right) + B\left[\frac{[\mathrm{erf}(qR_g/\sqrt{6})]^3}{q}\right]^4 \right\} S(q) \quad (1)$$

where $R_g$ is the Guinier average of the radius of gyration of the isolated particles.[40] For a two-electron density model, $G$ and $B$

**TABLE 2: $^{29}$Si MAS NMR Population (±5%) of the Different $T^i$ Species and Degree of Condensation, *C*, of the Selected d-U(600)$_n$Nd(CF$_3$SO$_3$)$_3$ Di-ureasils and d-Ut(300)$_n$Nd(CF$_3$SO$_3$)$_3$ and d-Ut(600)$_n$Nd(CF$_3$SO$_3$)$_3$ Di-urethanesils**

| | d-U(600)$_n$Nd(CF$_3$SO$_3$)$_3$ | | | | d-Ut(300)$_n$Nd(CF$_3$SO$_3$)$_3$ | | | | d-Ut(600)$_n$Nd(CF$_3$SO$_3$)$_3$ | | | |
|---|---|---|---|---|---|---|---|---|---|---|---|---|
| *n* | $T^1$ (%) | $T^2$ (%) | $T^3$ (%) | *c* (%) | $T^1$ (%) | $T^2$ (%) | $T^3$ (%) | *c* (%) | $T^1$ (%) | $T^2$ (%) | $T^3$ (%) | *c* (%) |
| 200 | 9 | 41 | 51 | 81 | 16 | 31 | 53 | 79 | <3 | 30 | 69 | 89 |
| 80 | | | | | 14 | 31 | 55 | 80 | <3 | 30 | 69 | 89 |
| 40 | 9 | 42 | 49 | 80 | | | | | | | | |

are given by $G = N(\rho_p - \rho_m)^2 v^2$ and $B = 2\pi(\rho_p - \rho_m)^2 S$, where $N$ is the number of particles per unit volume, $v$ is the particle volume, $S$ is the interface area between the particles and the matrix and $\rho_p$ and $\rho_m$ are average electron densities of the particles and the matrix, respectively. Since the SAXS curves of the d-Ut(300) samples do not demonstrate the Porod law behavior within the studied range, the corresponding term was omitted in its analysis. This implies that in these hybrids $R_g$ is not well-defined. The structure−function $S(q)$ for spherical particles, in which the only correlation is a hard sphere interaction, is given by

$$S(q) = 1/(1 + k\theta) \quad (2)$$

where $k = 8V/V_0$, is the packing factor, $V$ is the average "hard-core" volume, and $V_0$ is the average available volume to each sphere. The $\theta$ factor depends on the average intersphere distance $d$ as follows: $\theta = 3[\sin(qd) - qd\cos(qd)]/(qd)^3$

The best fits of eq 1 to the medium and high $q$ regions of the experimental SAXS curves are displayed as continuous lines in Figure 6. The relevant structural parameters obtained from fit procedure are displayed in Table 3. Globally, we notice in the three sets of scattering curves that the position of the maximum strongly depends on the length of the polymer chains (e.g., for the d-Ut(300)$_n$Nd(CF$_3$SO$_3$)$_3$ and d-Ut(600)$_n$Nd-(CF$_3$SO$_3$)$_3$ di-urethanesil materials $q_{max}$ is about 0.34 and 0.23 Å$^{-1}$, respectively). This implies that, as expected in the light of the proposed model, the average distance $d$ is higher for the d-Ut(600)$_n$Nd(CF$_3$SO$_3$)$_3$ materials (∼ 19 Å) than for d-Ut(300)$_n$Nd(CF$_3$SO$_3$)$_3$ hybrids (∼ 16 Å) (Table 3).

Concerning the influence of the nature of the polymers (urea or urethane cross-links) we remark that the average distance between siloxane clusters does not vary strongly. For the d-U(600)$_n$Nd(CF$_3$SO$_3$)$_3$ system, we have determined larger distances than for the d-Ut(600)$_n$Nd(CF$_3$SO$_3$)$_3$ family (Table 3). The existence of more $CH_2CH_2O$ repeating units (13) in d-Ut(600) than in d-U(600) (8.5) is balanced by the existence of $CH(CH_3)CH_2O$ (2.5) and $CH(CH_3)CH_2$ (1) units. Therefore, the larger $d$ values found in the d-U(600)-based hybrids reflect the existence of different monomer units and chain conformations. As it will be described below, the effects of the addition of $Nd^{3+}$ are globally similar but not the same for the three studied systems.

In the case of the d-U(600)$_n$Nd(CF$_3$SO$_3$)$_3$ system, both $d$ and $k$ are essentially invariant with salt content (Table 3). At the same time $R_g$ decreases with the increase of doping. The following facts suggest a model where $N$ increases with the increase of salt concentration: (1) the number of silicon atoms is essentially equal for all $Nd^{3+}$ concentrations, (2) $R_g$ decreases with doping, and (3) no monomeric $T^0$ silicon species occur (Figure 5). The fact that $k$ remains constant indicates that there are no significant changes in the interdomain order. In this model, the $Nd^{3+}$ ions might be regarded as siliceous domain nucleation agents, meaning that the lanthanide ions either promote the creation of a higher number of siloxane clusters or inhibit the growth/coalescence of the clusters initially formed. We must emphasize that the FT-IR and Raman spectroscopic data discussed above show the interaction between the $Nd^{3+}$ ions and the urea groups located on the siliceous domains surface. The influence of the $Nd^{3+}$ ions on the d-U(600) matrix is quite different from that of the $Eu^{3+}$ ions: with the latter cations, $Eu^{3+}$/urea and $Eu^{3+}$/POE interactions were discerned and their formation was found to be dependent on the $Eu^{3+}$ concentration; however, no increase of the siliceous domains density was observed.[41]

The SAXS structural parameters corresponding to the d-Ut(600) system (Table 3) exhibit a decrease of $d$, $k$, and $R_g$ as the $Nd^{3+}$content increases. Similar to what happens in the

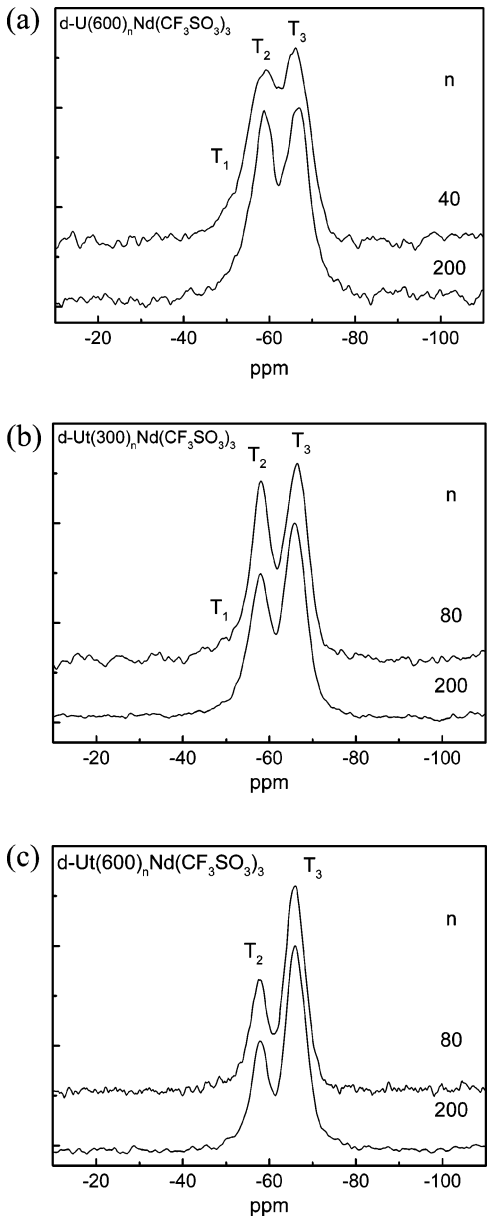


**Figure 5.** $^{29}$Si MAS NMR spectra for selected $Nd^{3+}$ concentrations of the (a) d-U(600)$_n$Nd(CF$_3$SO$_3$)$_3$ di-ureasils and (b) d-Ut(300)$_n$Nd-(CF$_3$SO$_3$)$_3$ and (c) d-Ut(600)$_n$Nd(CF$_3$SO$_3$)$_3$ di-urethanesils.

**TABLE 3: Average Intersiloxane Particles Distance, *d*, Packing Factor *k*, *G* Constant, and Average Gyration Radius $R_g$ for d-U(600)$_n$Nd(CF$_3$SO$_3$)$_3$ Di-ureasils and d-Ut(300)$_n$Nd(CF$_3$SO$_3$)$_3$ and d-Ut(600)$_n$Nd(CF$_3$SO$_3$)$_3$ Di-urethanesils, Obtained with the Fit Procedure**

| | d-U(600)$_n$Nd(CF$_3$SO$_3$)$_3$ | | | d-Ut(300)$_n$Nd(CF$_3$SO$_3$)$_3$ | | | | d-Ut(600)$_n$Nd(CF$_3$SO$_3$)$_3$ | | |
|---|---|---|---|---|---|---|---|---|---|---|
| | $n = 400$ | $n = 200$ | $n = 40$ | $n = 200$ | $n = 100$ | $n = 80$ | $n = 60$ | $n = 200$ | $n = 100$ | $n = 80$ |
| $d$ ($\pm$0.2 Å) | 24.2 | 24.5 | 24.0 | 16.9 | 16.7 | 16.1 | 15.6 | 19.4 | 18 | 18 |
| $k$ ($\pm$0.2) | 4.2 | 4.4 | 4.3 | 3.6 | 3.7 | 3.3 | 2.2 | 1.6 | 1.3 | 0.6 |
| $R_g$ ($\pm$1 Å) | 8.7 | 5 | 4.8 | | | | | 5.1 | 4.7 | 4 |

d-U(600) hybrids, this trend can be understood considering that an increase of the siliceous domains number, *N*, and an increase of the interdomain disorder occur in parallel. In fact, the disorder of the $Nd^{3+}$-doped d-Ut(600) matrices is in accordance with the spectroscopic results presented above that established that the POE became more disordered upon introduction of the neodymium salt. At the same time, the existence of $Nd^{3+}$ urethane interactions inferred from FT-IR spectra and thus the presence of $Nd^{3+}$ ions on the siliceous domains surface is in accordance with the effect of these cations on the domains nucleation.

Finally, the overall characteristics of the d-Ut(300)$_n$Nd(CF$_3$SO$_3$)$_3$ system SAXS curves (Figure 6c) are similar to those of the d-Ut(600)$_n$Nd(CF$_3$SO$_3$)$_3$ family: the relative amplitude of the correlation peak gradually decreases and shifts to higher

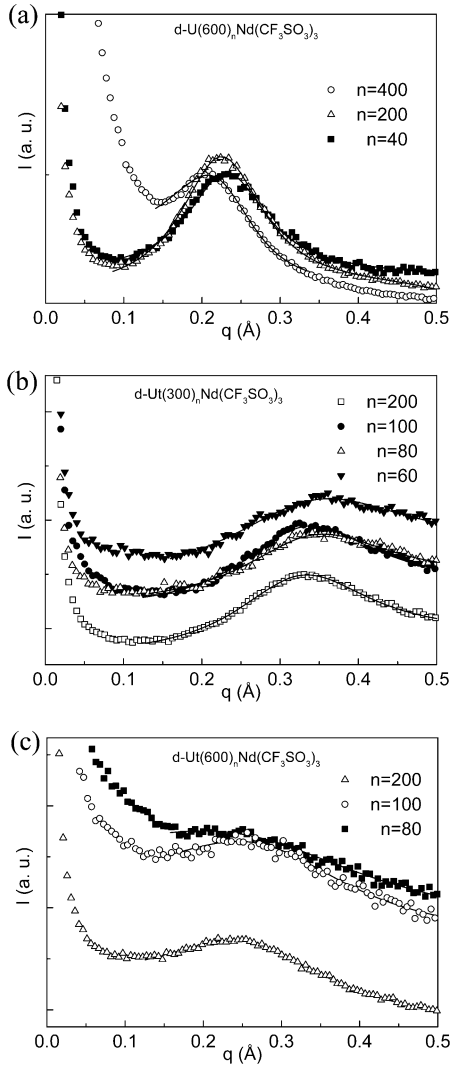


**Figure 6.** Experimental SAXS curves corresponding to (a) d-U(600)$_n$Nd(CF$_3$SO$_3$)$_3$, (b) d-Ut(600)$_n$Nd(CF$_3$SO$_3$)$_3$, and (c) d-U(600)$_n$Nd(CF$_3$SO$_3$)$_3$ hybrids with different $Nd^{3+}$ doping levels. Continuous lines represent the results of fitting the experimental curves with eq 1.

*q* values and the average intercluster distance decreases at increasing $Nd^{3+}$ content while the packing factor *k* decreases (Table 3). Thus, the $Nd^{3+}$ ions affect the siliceous domains order, a finding that is agreement with the presence of $Nd^{3+}$/urethane interactions. As in the case of the d-Ut(600) system, the spectroscopic results obtained for the d-Ut(300)$_n$Nd(CF$_3$SO$_3$)$_3$ analogues showed that the POE chains order is affected by the $Nd^{3+}$/urethane coordination, an effect related with the decrease of *k*. This disorder effect, which does not involve $Nd^{3+}$/POE interactions, highlights the importance of the POE/urethane and urethane/urethane interactions on the POE chains arrangement and on the order of the interdomain nanostructure of the undoped d-Ut(*Y*)-based matrices.

**Photoluminescence Spectroscopy.** The RT PL features in the visible spectral range of a set of selected di-ureasil and di-urethanesil hybrids are represented in Figure 7, parts a−c, respectively. The spectra of the corresponding undoped hosts are also plotted to help our discussion. All the spectra are composed of a large broad band in the blue-green spectral regions (380−600 nm), which, for higher salt concentrations ($n \leq 20$), is overlapped by a series of straight self-absorptions assigned to intra-4f$^3$ transitions. This broad band was already observed in similar $Eu^{3+}$- and $Nd^{3+}$-based hybrids and in the corresponding undoped hosts. A systematic study involving steady-state and time-resolved PL and lifetimes of the undoped di-ureasils and di-urethanesils was performed previously, establishing the unequivocal presence of two emission components, attributed to radiative recombinations typical of donor−acceptor pairs, which occur in the NH groups of the urea or urethane cross-links (blue emission) and in the siliceous nanodomains (purplish-blue emission).[18,45−48] It was recently proposed that the mechanism responsible for the NH-related component is associated with photoinduced proton-transfer between $NH_2^+$ and $N^-$ defects, whereas the PL mechanism subjacent to the component associated with the siliceous nanodomains involves oxygen-related defects.[47]

Close analysis of the RT PL spectra of the di-urethanesil hybrids (Figure 7, parts b and c) allows one to infer that a minor blue-shift (0.11 eV) is observed with respect to the undoped host, readily indicating an effective interaction between the $Nd^{3+}$ ions and the hybrid host. Apart from the increase in the relative intensity between the intra-4f$^3$ self-absorptions and the broad band, no significant changes are observed in the energy and full-width at half-maximum (fwhm) of the emission band as the $Nd^{3+}$ concentration increases from $n = 200$ to 4. For the d-U(600)$_n$Nd(CF$_3$SO$_3$)$_3$ di-ureasil hybrids (Figure 7a) the incorporation of a small amount of $Nd^{3+}$ ($n = 200$) leads to a small blue-shift (0.11 eV) of the broad band maximum intensity, similarly to what is observed for the two di-urethanesil systems investigated here. However, upon further increase of the concentration up to $n = 20$ the maximum intensity of the large broad band shifts to the red region, overlapping the emission of the undoped host. The broad band emission energy for the most concentrated sample ($n = 5$) resembles again that observed for the hybrid with $n = 200$; i.e., the emission is red-shifted around 0.11 eV with respect to the undoped host. For the more

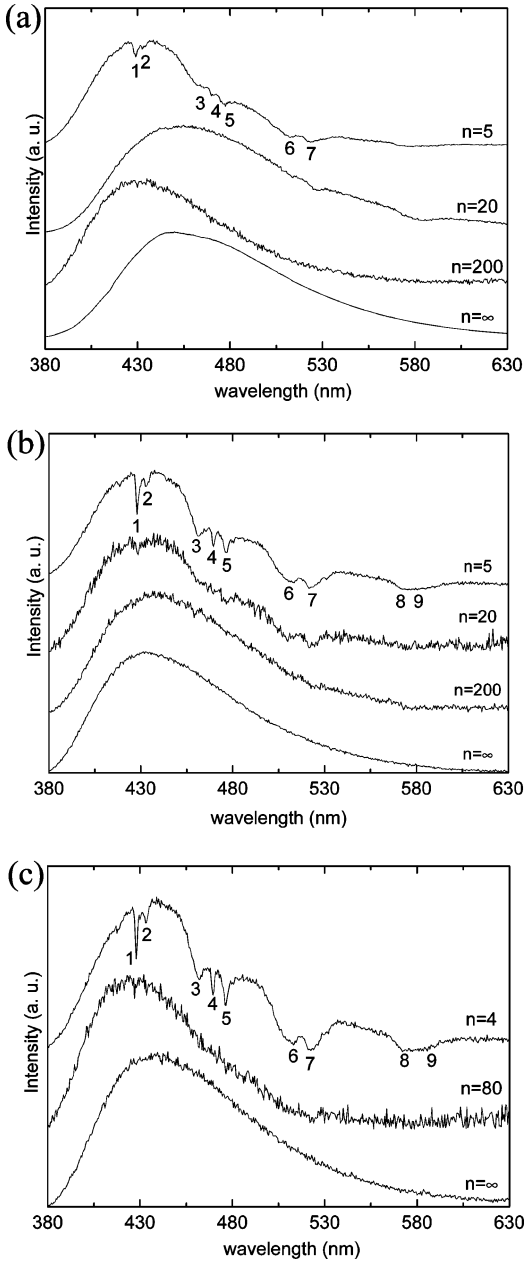


**Figure 7.** RT PL spectra obtained under 365 nm excitation wavelength for the (a) d-U(600)$_n$Nd(CF$_3$SO$_3$)$_3$ ($n = \infty$, 200, 20, 5) di-ureasils, (b) d-Ut(300)$_n$Nd(CF$_3$SO$_3$)$_3$ ($n = \infty$, 200, 20, 5), and (c) d-Ut(600)$_n$Nd-(CF$_3$SO$_3$)$_3$ ($n = \infty$, 80, 4) di-urethanesils. 1, 2, 3, 4, 5, 6, 7, 8, and 9 denotes the intra-4f$^3$ transitions: $^4I_{9/2} \rightarrow {}^2P_{11/2}$, $^2D_{5/2}$, $^2G_{9/2}$, $^4G_{11/2}$, $^2K_{15/2}$, $^4G_{7/2}$, $^2K_{13/2}$, $^4G_{7/2}$, $^2G_{7/2}$, respectively.

concentrated hybrids a series of intra-4f $^3$ self-absorptions is also discernible, the intensity of which increase as the ion content increases.

The PLE spectra was monitored along the hybrid host emission band for the d-U(600)$_n$Nd(CF$_3$SO$_3$)$_3$ di-ureasils. As Figure 8 shows, all the spectra are composed of a large broad band in the ultraviolet/visible spectral range. Similarly to what was reported for the emission, the PLE spectra of the most concentrated sample displays intra-4f$^3$ absorption lines. As the monitoring wavelength increases from 400 to 500 nm, the spectra get broader, indicating the presence of more than one PLE component. Such behavior was detected and interpreted in-depth for the other di-ureasil families.[48] The higher and lower energy sides of the PLE spectra were assigned to the preferential excitation of the NH- and siliceous-based excited states.[48] As

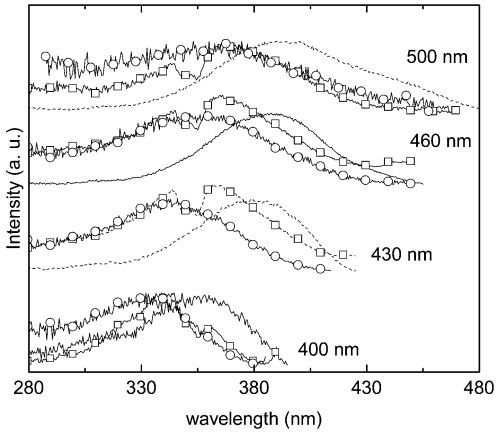


**Figure 8.** RT PLE spectra monitored at different monitoring wavelengths between 400 and 500 nm for the d-U(600)$_n$Nd(CF$_3$SO$_3$)$_3$ with (solid line and circles) $n = 200$, (solid line) $n = 20$ and (solid line and squares) $n = 5$.

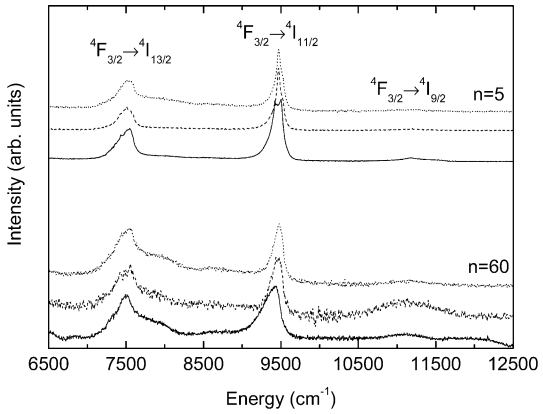


**Figure 9.** RT near-infrared spectra excited at 514.5 nm for the (solid) d-U(600)$_n$Nd(CF$_3$SO$_3$)$_3$ di-ureasils, (dashed) d-Ut(600)$_n$Nd(CF$_3$SO$_3$)$_3$ and (dotted) d-Ut(300)$_n$Nd(CF$_3$SO$_3$)$_3$ di-urethanesils, with $n = 60$ and 5.

the spectrum of the di-ureasil with $n = 20$ is red-shifted with respect to the remaining di-ureasil hybrids (as was observed in PL; see Figure 7a), this might indicate that the emission associated with the NH groups has a larger contribution than that observed in the other di-ureasils.

The appearance of intra-4f $^3$ self-absorptions both in the PL and PLE spectra has already been observed in longer polymer chain di-ureasils, and it was interpreted as a signal of intra-Nd$^{3+}$ conversion process of visible light into infrared luminescence.[9,10] In fact, the di-urethanesils and di-ureasils discussed here show efficient RT PL in the near-infrared spectral region, assigned to intra-4f $^3$ transitions between the $^4F_{3/2}$ and the $^4I_{9/2,11/2,13/2}$ levels. Figure 9 exemplifies the infrared PL for the two selected samples of each series of di-ureasils and di-urethanesils. No significant changes are observed in the energy and fwhm of the lines in the different hosts and with increasing concentration from $n = 200$ to 20. In the case of the most concentrated Sample $n = 5$ the profile of the Nd$^{3+}$ transitions, in particular the $^4F_{3/2} \rightarrow {}^4I_{11/2}$, gets more structured. Moreover, we can refer, in a qualitatively way, that no quenching effects due to increasing concentration were detected, as the experimental conditions (excitation power and detection slits) were kept constant during the entire set of measurements. The observation of RT PL from the Nd$^{3+}$ ions is not common in organic/inorganic hybrids due to the presence of numerous organic groups, particularly the hydroxy group that act as nonradiative channels for the excited levels of the Nd$^{3+}$ ions.[8−10]

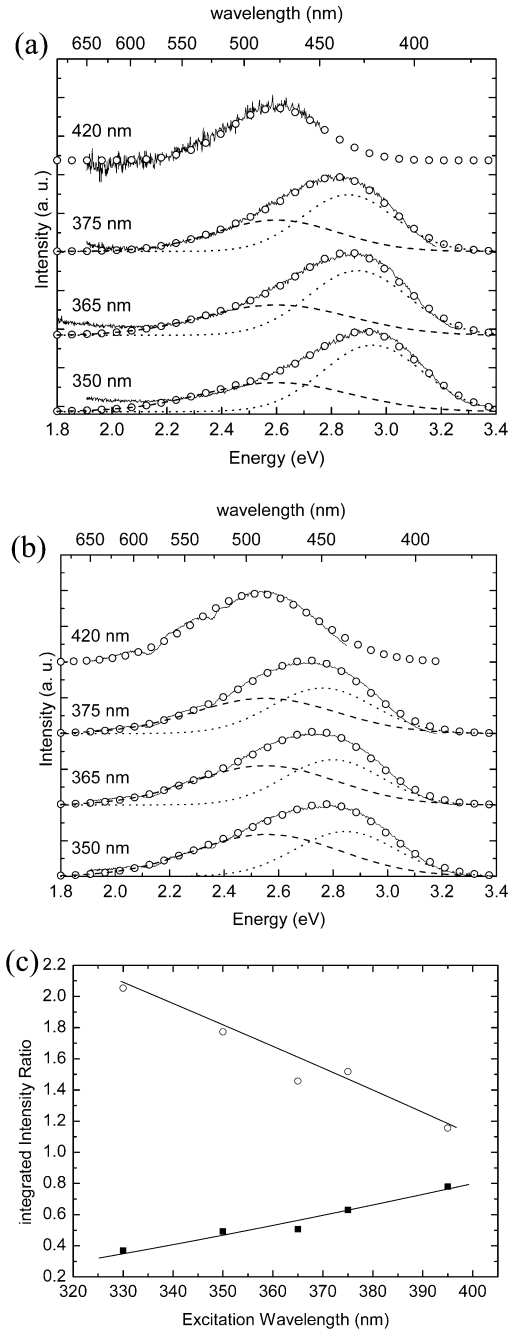


**Figure 10.** RT PL spectra excited at different monitoring wavelengths between 350 and 420 nm for the d-U(600)$_n$Nd(CF$_3$SO$_3$)$_3$ (a) $n = 200$ and (b) $n = 20$, and the respective Gaussian peak functions resulting from the fitting procedure: (dashed line) NH-related component, (dotted line) siliceous-related component and (open circles) fit envelope. (c) Ratio between the integrated intensity of the two components for the two previous samples as a function of the excitation wavelength.

The most noticeably differences between the $Nd^{3+}$-based di-ureasils and di-urethanesils are the energetic differences between the undoped host and the doped hybrids. This is particularly true for the d-U(600)$_n$Nd(CF$_3$SO$_3$)$_3$ hybrids whose energetic shift with respect to the undoped d-U(600) host is concentration dependent. To gain some insight into the PL description, specially to quantify the energy, fwhm, and the relative intensity between the NH- (blue band) and siliceous- (purplish-blue band) related PL components of such hybrids, we performed a deconvolution fitting procedure to the PL spectra excited within the excitation interval between 330 and 420 nm for two hybrids with $n = 200$ and $n = 20$ (Figure 10, parts a and b). The samples at higher concentrations ($n < 20$) were excluded from this analysis due to the higher relative intensity between the intra-4f $^3$ self-absorptions and the hybrid host emission that distorts the band envelope disabling a correct fitting procedure. The method used was similar to that previously applied to the undoped host.[45−47] One Gaussian function was used to fit the emission spectrum excited at 420 nm (2.95 eV). Since the fwhm is determined primarily by carrier-phonon interaction, its value should not be affected by the variation of the excitation energy. Therefore, for each hybrid, the blue and purplish-blue fwhm-fitted values were considered to be independent of the excitation energy. In contrast, the peak energies and their integrated intensity were, for each hybrid, free to vary for the whole excitation energy range used. For excitation wavelengths between 330 and 400 nm (3.10−4.00 eV) the fitting method revealed the presence of two Gaussian bands in the blue (≈2.55−2.60 eV) and in the purplish-blue (2.74−2.93 eV) spectral regions. Only the former component was observed for excitation wavelengths in the 400−420 nm (2.95−3.10 eV) interval. The fwhm reached approximately 0.50 and 0.40 eV for the blue and purplish-blue bands, respectively. The most notorious variations found in the fitting parameters are related with variations in the integrated intensity of the two PL components and in the energy as the concentration increases from $n = 200$ to 20. Figure 10c shows the ratio between the integrated intensity of the NH-related emission and that correspondent to the siliceous nanodomains. We note that the emission associated with the NH groups contributes with lower efficiency for the PL features of the hybrid with $n = 200$, with respect to the band associated with the siliceous domains. For the more concentrated sample ($n = 20$), the opposite situation occurs. This conclusion was derived also from the analyses of the PLE spectra.

The smaller contribution of the NH groups to the PL features of the d-U(600)$_{200}$Nd(CF$_3$SO$_3$)$_3$ samples with respect to d-U(600)$_{20}$Nd(CF$_3$SO$_3$)$_3$ may be correlated with the stronger hydrogen-bonded associations established, as pointed out above in the section devoted to cation/cross-link interactions. The presence of stronger hydrogen bonds contributes to localize the proton rendering difficult the induced transfer of hydrogen atoms between NH groups and, consequently, the NH-related emission will be less intense in the sample with $n = 200$.

## Conclusions

The sol−gel process was used to synthesize families of di-urea and di-urethane cross-linked POE/siloxane-based materials incorporating Nd(CF$_3$SO$_3$)$_3$. The analysis of the specific vibrational modes of the POE chains and of the urea and urethane cross-links provided evidences that in these materials the coordination of the lanthanide ions takes place in the following way: (1) at $n > 10$ for the d-U(600)$_n$Nd(CF$_3$SO$_3$)$_3$ di-ureasils and $n > 20$ for the d-Ut(300)$_n$Nd(CF$_3$SO$_3$)$_3$) and d-Ut(600)$_n$Nd-(CF$_3$SO$_3$)$_3$ di-urethanesils, the cations interact exclusively with the carbonyl oxygen atoms of the urea and urethane linkages, respectively; (2) at $n \leq 10$ for the d-U(600)$_n$Nd(CF$_3$SO$_3$)$_3$ di-ureasils and $n \leq 20$ for the d-Ut(300)$_n$Nd(CF$_3$SO$_3$)$_3$) and d-Ut(600)$_n$Nd(CF$_3$SO$_3$)$_3$ di-urethanesils, the coordination of the cations to the oxygen atoms of the polyether chains occurs. Thus, for low $Nd^{3+}$ concentrations the cation preferential coordination site is the carbonyl group located at the organic/inorganic interface, independently of the organic chain length and the nature of the cross-link. This $Nd^{3+}$/carbonyl group interaction affects the polycondensation of the siloxane species. In the d-U(600) and d-Ut(600) matrices the $Nd^{3+}$ cations act as

nucleation agents, since the size of the siloxane domains decreases with the $Nd^{3+}$ content. The siloxane domains are spatially correlated at a mean distance that depends mainly on the chain length and conformation. The formation of $Nd^{3+}$/carbonyl group interactions at the expense of the destruction of some POE/urethane and urethane/urethane interactions also influences the POE chains local order of the d-Ut(600) hybrids, promoting more disordered arrangements.

$Nd^{3+}$-based organic/inorganic hybrids present interesting RT PL features, due to the overlap of purple-blue-green and infrared luminescence, originating from recombinations occurring in the host matrix (NH groups of the urea linkages and siliceous domains) and from the $^4F_{3/2} \rightarrow {}^4I_{9/2-13/2}$ intra-$4f^3$ transitions, respectively. The relative contribution of the NH groups to the PL features may be induced by the formation of stronger hydrogen-bonded aggregates that contribute to localize the proton rendering difficult the induced transfer of hydrogen atoms between NH groups.

**Acknowledgment.** This work was supported by FEDER and Fundação para a Ciência e Tecnologia (POCTI/CTM/46780/02) and GRICES from Portugal, and FAPESP and CAPES from Brazil. The authors acknowledge the collaboration of LNLS staff. N.J.O.S. acknowledges a scholarship by FCT (SFRH/BD/10383/2002). The authors thank S. M. Gomes Correia for synthesizing the di-ureasil samples.

## References and Notes

(1) Brinker, C. J.; Scherer, G. W. *Sol−gel Science, The Physics and Chemistry of Sol−Gel Processing*; Academic Press: San Diego, CA, 1990.
(2) *Functional Hybrid Materials*, Gomez-Romero, P.; Sanchez, C. Eds.; Wiley-Interscience: New York, 2003.
(3) Sanchez, C.; Lebeau, B.; Chaput, F.; Boilot, J.-P. *Adv. Mater*. **2003**, *15*, 1969.
(4) Polman, A. "Erbium doped planar optical amplifiers," In *10th European Conference on Integrated Optical (ECIO)*; Paderborn, Germany, Apr. 2001, pp 75−79.
(5) Viana, B.; Cordoncillo, E.; Philippe, C.; Sanchez, C.; Javier Guaita, F.; Escribano, P. In *Proceedings of the SPIE*; The International Society for Optical Engineering: Bellingham, WA, 2000; Vol. 3943; pp 128−138.
(6) Lecomte, M.; Viana, B.; Sanchez, C. *J. Chem. Phys.* **1995**, *88*, 39.
(7) Viana, B.; Koslova, N.; Aschehoug, P.; Sanchez, C. *J. Mater. Chem.* **1995**, *5*, 719.
(8) Sanchez, C.; Ribot, F.; Lebeau, R. *J. Mater. Chem.* **1999**, *9*, 35.
(9) Carlos, L. D.; Sá Ferreira, R. A.; De Zea Bermudez, V. *Electrochim. Acta* **2000**, *45*, 1555.
(10) Sá Ferreira, R. A.; Carlos, L. D.; De Zea Bermudez, V.; Molina, C.; Dahmouche, K.; Messaddeq, Y.; Ribeiro, S. J. L. *J. Sol-Gel Sci. Technol.* **2003**, *26*, 315.
(11) Driesen, K.; Van Deun, R.; Görller-Walrand, C.; Binnemans, K. *Chem. Mater*. **2004**, *16*, 1531.
(12) Sun, L. N.; Zhang, H. J.; Fu, L.; Liu, F. Y.; Meng, Q. G.; Peng, C. Y.; Yu, J. B. *Adv. Func. Mater*. **2005**, *15*, 1041.
(13) Sun, L. N.; Zhang, H. J.; Meng, Q. G.; Liu, F. Y.; Fu, L.; Peng, C. Y.; Yu, J. B.; Zheng, G. L.; Wang, S. B. *J. Phys. Chem. B* **2005**, *109*, 6174.
(14) Nunes, S. C.; De Zea Bermudez, V.; Sá Ferreira, R. A.; Carlos, L.; Morales, E.; Marques, P. V. S. *Mater. Res. Soc. Symp. Proc.* **2005**, *847*, EE13.31.1.
(15) De Zea Bermudez, V.; Sá Ferreira, R. A.; Carlos, L. D.; Molina, C.; Dahmouche, K.; Ribeiro, S. J. L. *J. Phys. Chem. B* **2001**, *105*, 3378.
(16) De Zea Bermudez, V.; Ostrovskii, D.; Gonçalves, M. C.; Carlos, L. D.; Sá Ferreira, R. A.; Reis, L.; Jacobsson, P. *Phys. Chem. Chem. Phys.* **2004**, *6*, 638.
(17) De Zea Bermudez, V.; Ostrovskii, D.; Lavoryk, S.; Gonçalves, M. C.; Carlos, L. D. *Phys. Chem. Chem. Phys*. **2004**, *6*, 649.
(18) Gonçalves, M. C.; De Zea Bermudez, V.; Sá Ferreira, R. A.; Carlos, L. D.; Ostrovskii, D.; Rocha, J. *Chem. Mater*. **2004**, *16*, 2530.
(19) Silva, M. M.; De Zea Bermudez, V.; Carlos, L. D.; Smith, M. J. *Electrochim. Acta* **2000**, *45*, 1467.
(20) Peakfit is a product of Jandel Corporation, 2591 Rerner Boulevard, San Rafael, CA 94901.
(21) Bernson, A.; Lindgren, J. *Solid State Ionics* **1993**, *60*, 31.
(22) Bernson, A.; Lindgren, J.; Huang, W.; Frech, R. *Polymer* **1995**, *36*, 4471.
(23) Petersen, G.; Torell, L. M.; Panero, S.; Scrosati, B.; Silva, C. J.; Smith, M. J. *Solid State Ionics* **1993**, *60*, 55.
(24) Petersen, G.; Brodin, A.; Torell, L. M. *Solid State Ionics* **1994**, *72*, 165.
(25) Machida, K.; Miyazawa, T. *Spectrochim. Acta* **1964**, *20*, 1865.
(26) Matsuura, H.; Miyazawa, T. *J. Polym. Sci.* **1969**, *7* (A-2), 1735.
(27) Matsuura, H.; Miyazawa, T.; Machida, K. *Spectrochim. Acta* **1973**, *29A*, 771.
(28) Wendsjö, Å.; Lindgren, J.; Paluszkiewicz, C. *Electrochim. Acta* **1992**, *37*, 1689.
(29) Papke, B. L.; Ratner, M. A.; Shriver, D. F. *J. Phys. Chem. Solids* **1981**, *42*, 493.
(30) Papke, B. L.; Ratner, M. A.; Shriver, D. F. *J. Electrochem. Soc.* **1982**, *129* (7), 1434.
(31) Ericson, H.; Mattson, B.; Torell, L. M.; Rinne, H.; Sundholm, F. *Electrochim. Acta* **1998**, *43*, 1401.
(32) Furlani, M.; Ferry, A.; Franke, A.; Jacobsson, P.; Mellander, B.-E. *Solid State Ionics* **1998**, *113−115*, 129.
(33) Maxfield, J.; Shepherd, I. W. *Polymer* **1975**, *16*, 505.
(34) Matsuura, H.; Fukuhara, K. *J. Mol. Struct.* **1985**, *126*, 251.
(35) Gonçalves, M. C.; De Zea Bermudez, V.; Ostrovskii, D. Unpublished results.
(36) Skrovanek, D. J.; Howe, S. E.; Painter, P. C.; Coleman, M. M. *Macromolecules* **1985**, *18*, 1676.
(37) Coleman, M. M.; Lee, K. H.; Skrovanek, D. J.; Painter, P. C. *Macromolecules* **1986**, *19*, 2149.
(38) De Zea Bermudez, V.; Carlos, L. D.; Alcácer, L. *Chem. Mater*. **1999**, *11* (3), 569.
(39) Dahmouche, K.; Santilli, C. V.; Pulcinelli, S. H.; Craievich, A. F. *J. Phys. Chem B* **1999**, *103*, 4937.
(40) *Small-Angle Scattering of X-ray*, Glatter, O.; Kratky, O. Eds.; Academic Press: New York, 1982.
(41) Dahmouche, K.; Carlos, L. D.; De Zea Bermudez, V.; Sá Ferreira, R. A.; Santilli, C. V.; Craievich, A. F. *J. Mater Chem.* **2001**, *11*, 3249.
(42) Silva, N. J. O.; Dahmouche, K.; Santilli, C. V.; Amaral, V. S.; Carlos, L. D.; De Zea Bermudez, V.; Craievich, A. F. *J. Appl. Crystallogr.* **2003**, *36*, 961.
(43) Beaucage, G. *J. Appl. Crystallogr.* **1995**, *28*, 717.
(44) Beaucage, G.; Ulibarri, T. A.; Black, E. P.; Shaefer, D. W. Hybrid Organic−Inorganic composites. *ACS Symp. Ser*. **1995**, *97*, 585.
(45) Carlos, L. D.; Sá Ferreira, R. A.; De Zea Bermudez, V.; Ribeiro, S. J. L. *Adv. Funct. Mater*. **2001**, *11* (2), 111.
(46) Carlos, L. D.; Sá Ferreira, R. A.; De Zea Bermudez, V. In *Handbook of Organic−Inorganic Hybrid Materials and Nanocomposites*; Nalwa, H. S., Ed; American Scientific Publishers: Morth Lewis Way, CA, 2003; Vol. 1; Chapter 9, p 353−380.
(47) Carlos, L. D.; Sá Ferreira, R. A.; Pereira, R. N.; Assunção, M.; De Zea Bermudez, V. *J. Phys. Chem. B* **2004**, *108*, 14924.
(48) Sá Ferreira, R. A.; Carlos, L. D.; Gonçalves, R. R.; Ribeiro, S. J. L.; De Zea Bermudez, V. *Chem. Mater*. **2001**, *13*, 2991.